iScience

CellPress

Article

Voltage Does Not Drive Prestin (SLC26a5) Electro-Mechanical Activity at High Frequencies Where Cochlear Amplification Is Best

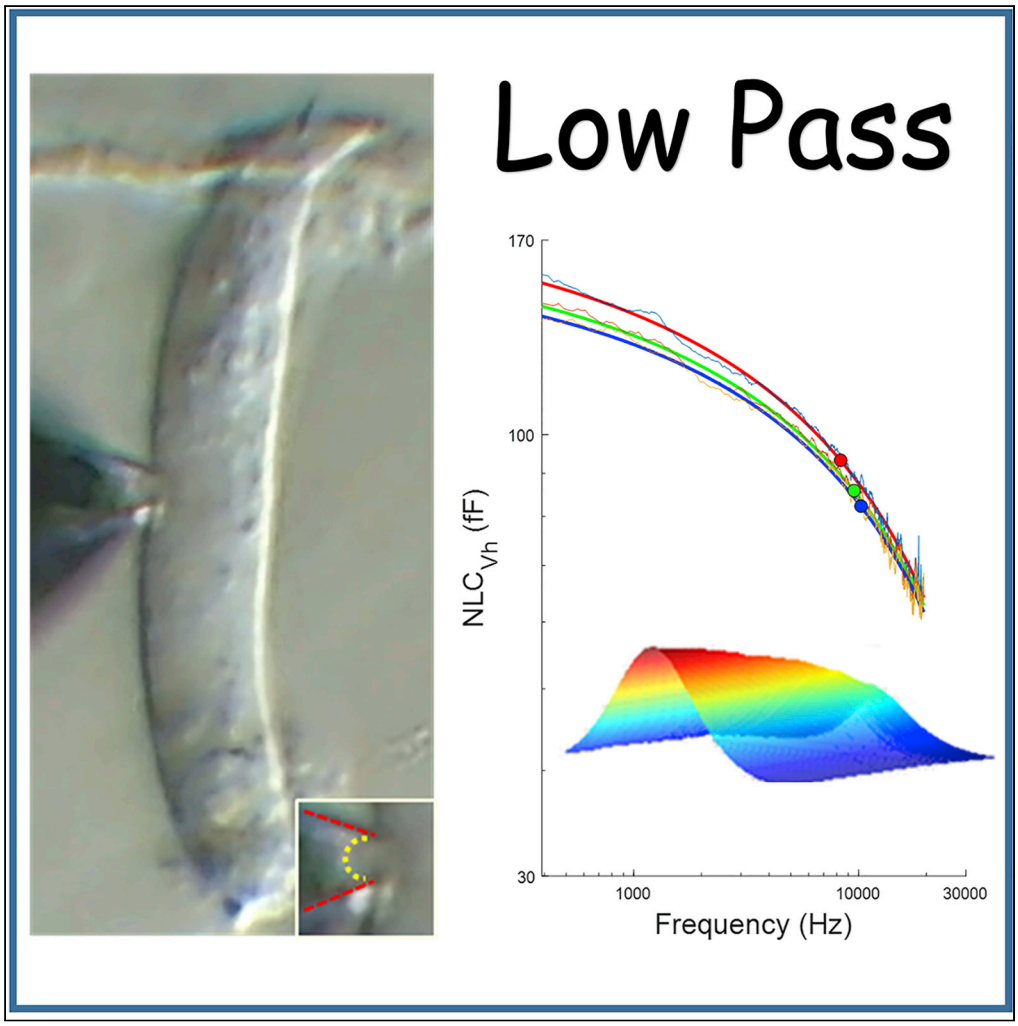

Joseph Santos-Sacchi, Winston Tan

joseph.santos-sacchi@yale.edu

HIGHLIGHTS

Outer hair cells (OHC) boost auditory sensation for very high acoustic frequencies

We studied the frequency response of OHC's electromechanical nonlinear capacitance

The response is incommensurate with cycle-by-cycle feedback at very high frequencies

OHCs likely use another mechanism to drive cochlear amplification at high frequencies

Santos-Sacchi & Tan, iScience *22*, 392–399
December 20, 2019
https://doi.org/10.1016/j.isci.2019.11.036

iScience

CellPress

Article

Voltage Does Not Drive Prestin (SLC26a5) Electro-Mechanical Activity at High Frequencies Where Cochlear Amplification Is Best

Joseph Santos-Sacchi[1,2,3,4,*] and Winston Tan[1]

SUMMARY

Cochlear amplification denotes a boost to auditory sensitivity and selectivity that is dependent on outer hair cells from Corti's organ. Voltage-driven electromotility of the cell is believed to feed energy back into the cochlear partition via a cycle-by-cycle mechanism at very high acoustic frequencies. Here we show using wide-band macro-patch voltage-clamp to drive prestin, the molecular motor underlying electromotility, that its voltage-sensor charge movement is unusually low pass in nature, being incapable of following high-frequency voltage changes. Our data are incompatible with a cycle-by-cycle mechanism responsible for high-frequency tuning in mammals.

INTRODUCTION

In some mammalian species, hearing capabilities can extend out to 60–160 kHz (Heffner and Masterton, 1980; Castellote et al., 2014; Szymanski et al., 1999; Heffner et al., 2001). Indeed, tuned hair cell receptor potential-derived cochlear microphonic potentials have been measured beyond 60 kHz in the bat (Pollak et al., 1972). Underlying this electrical behavior are sharp frequency tuning and enhanced cochlear partition vibration, which are susceptible to outer hair cell (OHC) damage; studies in laboratory rodents provide such evidence, e.g., in the mouse sharp basilar membrane tuning is measurable beyond 60 kHz (MelladoLagarde et al., 2008). This enhancement over Bekesy's passive partition vibration (von Bekesy, 1960) is termed cochlear amplification (CA) (Davis, 1983) and amounts to an apparent gain of 100–1000 at best frequency locations along the cochlear duct. DC and AC trans-membrane voltages are sensed by the membrane protein prestin (SLC26a5) (Santos-Sacchi and Dilger, 1988; Iwasa and Kachar, 1989), a special member of the SLC26 family of anion transporters (Zheng et al., 2000), that populates the OHC lateral membrane at molecular densities up to 8,000/μm^2 (Santos-Sacchi et al., 1997; Gale and Ashmore, 1997b). Voltage is thought to faithfully govern prestin's conformational state, evoking rapid switching between expanded and contracted molecular conformations that leads to rapid length changes (termed electromotility; eM) (Ashmore et al., 2010). Current dogma has it that evoked OHCeM provides mechanical feedback into the organ of Corti on a cycle-by-cycle basis to power CA. In fact, Frank et al. measured high-fidelity OHC AC eM responses beyond 80 kHz (Frank et al., 1999). During the last few years, however, the kinetics or frequency dependence of prestin's electromechanical capabilities have been reassessed in OHCs (Santos-Sacchi and Song, 2014; Santos-Sacchi, 2019). Both the frequency of prestin charge movement (measured as a nonlinear capacitance [NLC]) and that of its associated eM were found to be low-pass, precipitously rolling off within the bandwidth of human speech (200–8000 Hz) (Santos-Sacchi and Tan, 2018; Santos-Sacchi et al., 2019). However, those data must be viewed cautiously because measures were made in whole cell mode. In fact, being a piezoelectric-like protein (Iwasa, 1993; Gale and Ashmore, 1994; Kakehata and Santos-Sacchi, 1995), where reciprocal influences of mechanical load and voltage are at play, whole cell measures of OHC electromechanical activity may fail to establish the actual frequency capabilities of prestin. Here we address this issue by measuring the frequency response of prestin's NLC with on-cell and excised macro-patches from the cell's lateral membrane where isolation from external whole cell loads can be achieved. The macro-patch is the preferred methodology to gauge fast charge movement in voltage sensitive membrane proteins (Lu et al., 1995). Our patch data in mouse and guinea pig show low pass, voltage-driven electromechanical behavior of the protein, whose frequency response alters over time but still falls far short of its expected influence on cochlear amplification at very high frequencies, leading us to question prestin's role in this process.

RESULTS

Our recording system response (Figures S1A andS1B), and results on an electrical model of a membrane patch (Figures S1C–S1F), confirming our capability to measure capacitance flat out to 20 kHz, is provided

[1]Surgery (Otolaryngology), Yale University School of Medicine, BML 224, 333 Cedar Street, New Haven, CT 06510, USA

[2]Neuroscience, Yale University School of Medicine, 333 Cedar Street, New Haven, CT 06510, USA

[3]Cellular and Molecular Physiology, Yale University School of Medicine, 333 Cedar Street, New Haven, CT 06510, USA

[4]Lead Contact

*Correspondence: joseph.santos-sacchi@yale.edu

https://doi.org/10.1016/j.isci.2019.11.036

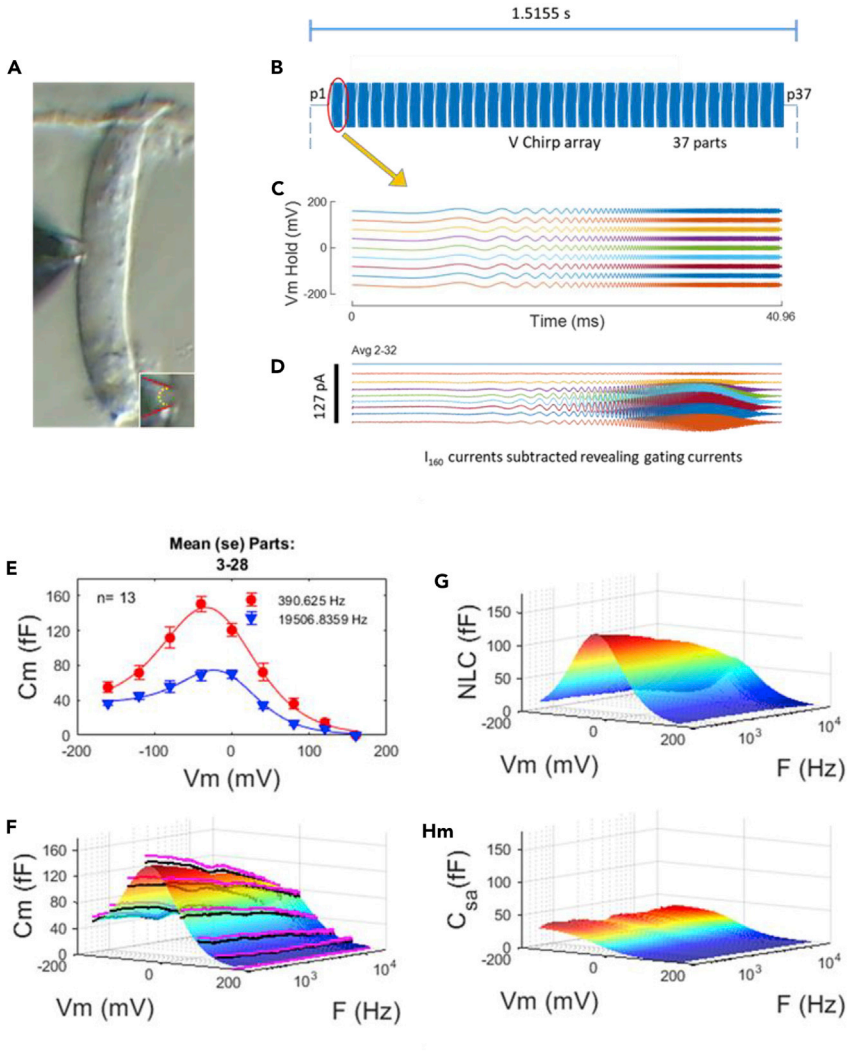

Figure 1. Measures of NLC in Macro-Patches from Outer Hair Cells (OHC)

(A) An image of an OHC (10 μm wide) showing a patch pipette sealed to the lateral membrane. Inset: enlarged view of patch. Red lines outline pipette, dotted yellow line outlines membrane patch.

(B) Section of command voltage stimulus, composed of 35 repeats of a chirp stimulus of 10 mV peak.

(C) Expanded view of individual chirp stimuli at the range of holding potential delivered to the patch (−160 to 160 mV).

(D) Extracted AC displacement ("gating") currents, representative of voltage sensor charge movements during conformational changes in prestin. Evoked raw currents at each holding potential were averaged from parts 2–32, then the averaged current at 160 mV, where prestin activity is absent, was subtracted from all raw currents at each holding potential, revealing prestin displacement currents. Here, for illustration, we plot the average of currents from all cells, but for subsequent data analysis each cell was individually analyzed to provide statistics. The magnitude of AC currents peaks near V_h, where prestin charge movement vs. voltage is maximal. The displacement currents were used to analyze for nonlinear capacitance (NLC).

(E) Extracted membrane capacitance at two stimulating frequencies, (390 Hz [red circles]) and 19,500 Hz [blue triangles]). Mean ± SE. Solid lines are fits based on Equation 1 (see Methods).

(F) Membrane capacitance as a function of voltage and frequency. Black lines are averages from 13 patches, and pink lines show mean +SE. Smooth multicolored surface is fit to averaged data.

(G) Extracted NLC. Note the roll-off in peak NLC magnitude as frequency of stimulation increases from 390 to 20,000 Hz.

(H) C_{sa} component of fit. Note frequency independence.

in the Transparent Methods section of the supplement. Figures1A–1D illustrate our basic experimental strategy. Macro-patches (3.5–4 μm inner diameter) were made on the lateral membrane of OHCs (Figure 1A) and a voltage chirp array delivered to the patch superimposed on stepped holding voltages (−160 to 160 mV) to

extract prestin displacement currents (Figure 1D), following subtraction of currents at +160 mV where NLC is absent (Santos-Sacchi and Navarrete, 2002). Single-sine or dual-sine admittance analysis of the displacement currents provides estimates of NLC. Figure 1E shows average (+/− SE) cell capacitance data fitted with Equation 1 (see Methods) at 2 frequencies (390 and 19,500 Hz). Note the substantial drop in peak membrane capacitance at the higher frequency. Figure 1F displays in a 3D rendition all frequencies studied across holding voltage. Black lines are average data and pink lines are mean +SE, whereas the multicolored plot shows fits. The extracted NLC is shown in Figure 1G and illustrates the continuous roll-off of NLC with increasing frequency. Figure 1H shows the largely frequency independent component of membrane capacitance (C_{sa}) at negative holding potentials that we previously attributed to membrane surface area/thickness changes during prestin's conformational changes between compact and expanded states (Santos-Sacchi and Navarrete, 2002). The clear roll-off differences between NLC and this C_{sa} response (Figures 1G and 1H) indicate that our previous interpretation of the C_{sa} component may need reevaluation.

NLC at V_h reflects the charge distribution where an equal amount of voltage sensor charge resides on either side of the plasma membrane. Furthermore, that characteristic voltage (V_h) is a reflection of the ratio of forward and backward rates of prestin transitions, providing a voltage at which to measure the characteristic rate or frequency of sensor charge movement. The coupling of charge movement and eM (Santos-Sacchi and Tan, 2018) also indicates that at this voltage OHCeM gain (cell length change/membrane potential) is maximal. In Figure 2A, we plot the frequency response of NLC at V_h (mean: blue line; mean +SE: light blue dotted line). The roll-off is precipitous commencing at the lowest measured frequency. It is clear that our data, collected at 24.4 Hz resolution, requires a multi-Lorentzian (double in this case), or a power function fit (Figure 2B). The double Lorentzian fit indicates a slow and fast component with frequency cut-offs (Fc) at about 1.5 and 16.2 kHz, respectively. For the power fit, we estimate a cut-off at one-half magnitude of 11.3 kHz. Figure 2C indicates that the frequency response of NLC is the same with on-cell or immediately excised macro-patches in the guinea pig. In Figure 2D, we show that the frequency response of NLC in mouse patches is similar to that of the guinea pig. Half-magnitude cut-off of the power fit is at 10.5 kHz. For comparison, we plot the chloride dependent capacitance frequency response of GAT1 (triangles) (Lu et al., 1995), and its power function fit (green line), indicating that it is somewhat faster than the frequency response of prestin. The guinea pig response (pink line) is replotted in the figure along with scaled eM data (OHC 65: magenta solid line; OHC84: dashed magenta line) from Frank et al. (1999) (Figure 2A), showing that the speed of prestin conformational transitions falls far below OHC mechanical responses. In other words, the drive for eM (voltage-dependent conformational changes in prestin) does not correspond to their measured eM. Can NLC frequency response be augmented?

We have previously shown that NLC is not stationary in time (Santos-Sacchi et al., 2009). Step changes in voltage evoke initial rapid changes in NLC, which immediately alter in magnitude in a stretched exponential fashion, accompanied by shifts in V_h. In Figure 3, we explore the frequency response of NLC along the duration of our holding potential steps. Figure 3A shows the regions of chirp currents that were averaged for comparison. The extracted NLC from the three regions are shown in Figure 3B, and for the first region (p3-8) a red line is plotted along the slope of NLC at V_h across frequency. That same red line is recast onto the two other plots of regions p13–18 and p23-28, showing alterations in the frequency response of NLC as duration of the step increases. A quantification of the frequency responses is made in Figure 3C. Power fits indicate that low frequency components are reduced over time such that the frequency cut-off effectively increases over time. Figures 3D–3G plot the fitted parameters of the power fit across holding potential duration, showing reductions in NLC_0, and time-dependent changes in the power parameters that control frequency dependence, with frequency cut-offs increasing over time.

It has been observed that patch size can change during the course of experiments (Sokabe et al., 1991). It is unlikely that patch size alterations across the duration of our voltage protocol account for the changes in frequency responses that we find because such changes would likely alter the size of NLC across the full frequency range (e.g., see Figure 2D, where smaller mouse patches simply shift all components of NLC downward relative to guinea pig patches). Indeed, Figures 3H and 3I illustrate that NLC across holding potential duration exhibits shifts in V_h that correspond to the nonstationary behavior of NLC that we previously found (Santos-Sacchi et al., 2009), rather than changes in patch area.

Salicylate is a known intracellular blocker of NLC (Kakehata and Santos-Sacchi, 1996; Tunstall et al., 1995), working in a competitive fashion on chloride binding (Oliver et al., 2001). Chloride anions are *not* extrinsic

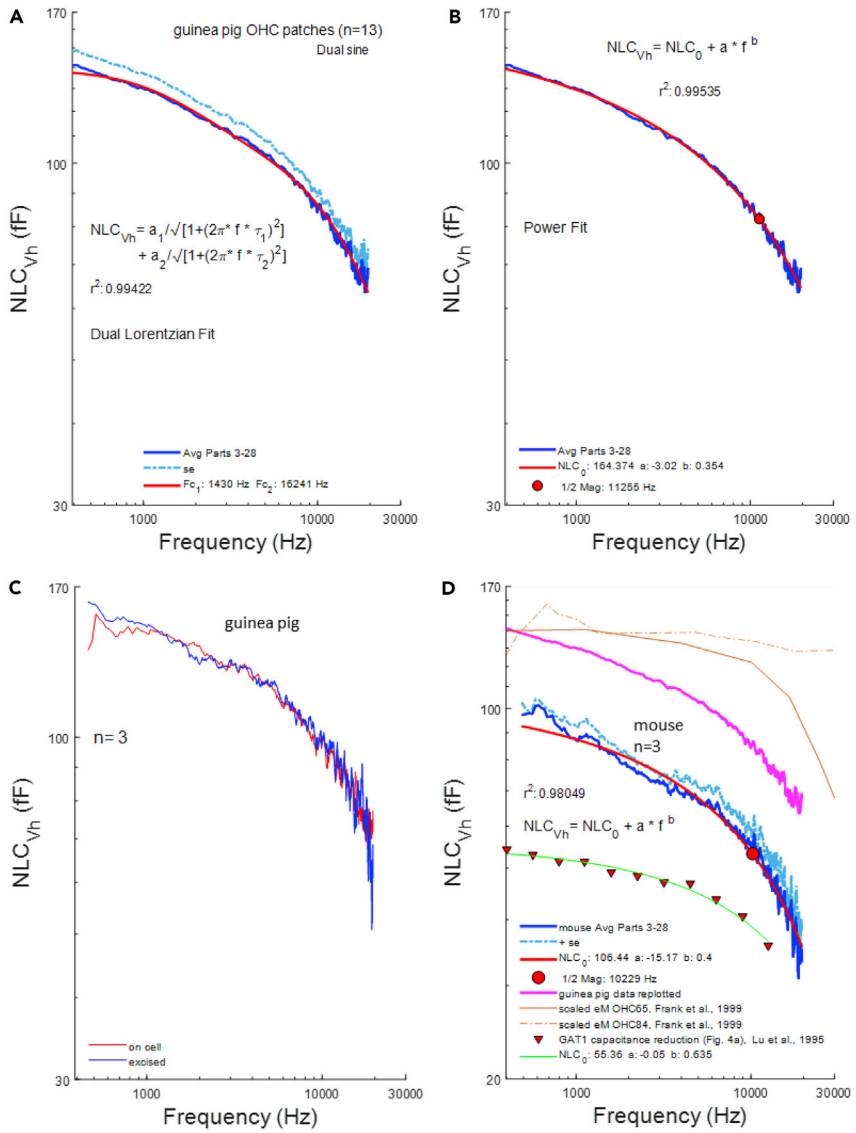

Figure 2. Frequency Response of NLC at V_h

(A) Blue line indicates mean NLC, dotted light blue line shows mean +SE. We require at least a double Lorentzian fit that indicates low and high pass components.

(B) Power fit of our data illustrating the continuous roll-off of NLC across frequency. One-half magnitude (red circle) is near 10.5 kHz.

(C) Average of three patches before and after inside-out patch excision, illustrating similar frequency response for each.

(D) Mouse NLC frequency response (mean, mean +SE, blue line, dotted light blue line, respectively) is similarly low pass compared with guinea pig response (pink line). Red circle shows one-half magnitude at 10.5 kHz. For comparison, we plot the capacitance function of Lu et al. (1995) (Figure 4A) for GAT1, fitted with a power function (solid green line). Also, for comparison, the scaled electromotility for the two presented cells from Frank et al. (1999) (Figure 2A) is shown. Note prestin's voltage-driven charge movements are remarkably lower-pass than eM.

voltage sensors for prestin but instead likely work allosterically (Song and Santos-Sacchi, 2010; Rybalchenko and Santos-Sacchi, 2003) (also see our comment #1 on Walter et al. [2019]—https://elifesciences.org/articles/46986). In Figure 4, we explore the effects of salicylate on NLC frequency response. Blue symbols denote responses after salicylate treatment, and red symbols denote response before treatment. Extracellular perfusion of high concentrations of salicylate (10 mM) substantially reduces NLC but not completely (Figure 4A). The effect results from intracellular loading of the ionized form of the molecule, working in the micromolar range (Kakehata and Santos-Sacchi, 1996). In order to gauge salicylate effects

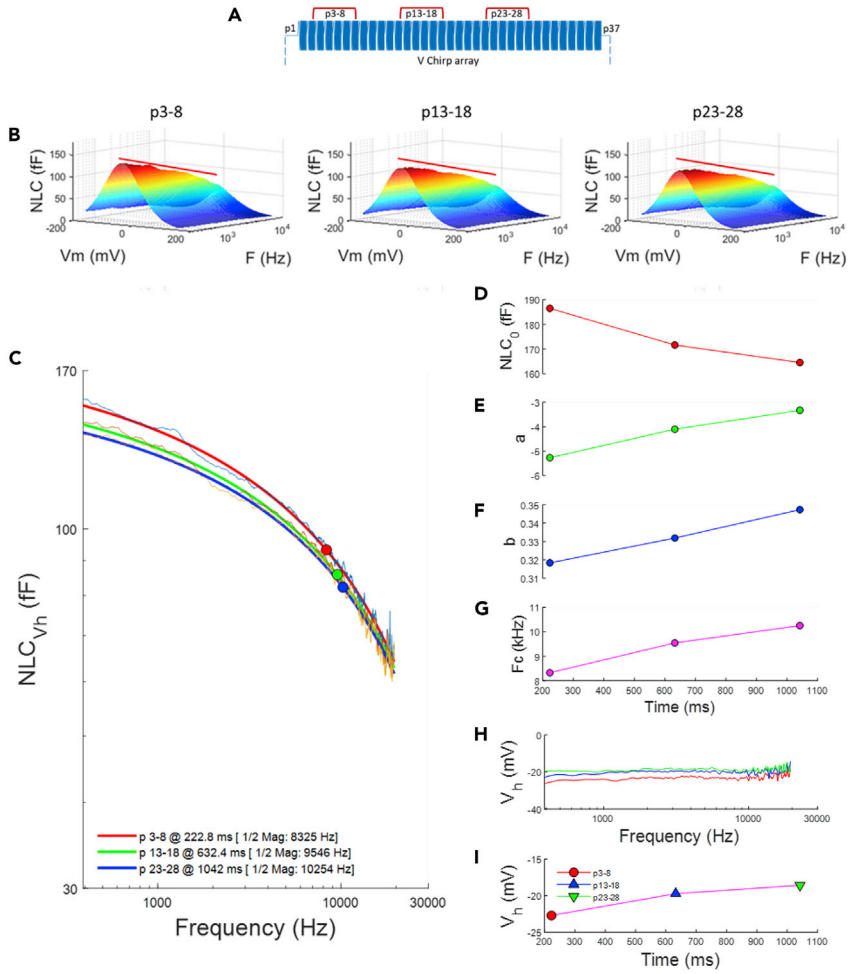

Figure 3. NLC Frequency Response Alters Over Time

(A) Currents were averaged at three time regions, six chirp responses each, over the duration of holding potential, p3-8, p13-18, and p23-28, and NLC was extracted for each region.

(B) NLC for the three durations is shown. The red line demarks the slope of NLC at V_h for the first region (p3-8) and is recast on the others. Note the change in NLC as duration of holding voltage increases.

(C) The frequency response of NLC at V_h is fit with a power function and shows that low-frequency regions of the response decreases over time. Circles depict one-half magnitude, which increases over time.

(D–G) Plots show the parameters of the power fits ([D] NLC_0, [E] a, [F] b, and [G] F_c) that alter over time.

(H and I) V_h shifts over the duration of holding voltage steps. (H) V_h across frequency (colors correspond to those in [C]).

(I) Mean V_h across frequency corresponding to data and colors in (H).

on NLC frequency response, we utilized lower concentrations (10 μM), assessing the response before (Figure 4B, *top panel*) and after (Figure 4B, *bottom panel*) treatment. Figure 4C shows that low-frequency components of NLC were reduced by 10 μM salicylate, effectively increasing the frequency cut-off. None of the NLC frequency modulations we observed, due to time dependence or salicylate interference with chloride binding, sufficiently increased the response to promote very high frequency electromechanical activity.

DISCUSSION

The identification of AC electromotile responses of the OHC (Kachar et al., 1986) offered a clue to the OHCs' ability to promote high-frequency enhancement of hearing in mammals (Dallos, 2008). The subsequent identification of the response's voltage dependence and associated voltage-sensor activity (Santos-Sacchi, 1990, 1991; Santos-Sacchi and Dilger, 1988; Ashmore, 1990) suggested that OHC receptor potentials, evoked by acoustic stimulation, drive feedback of mechanical energy into the cochlear partition. It is current dogma that this feedback is cycle-by-cycle, working best at high frequencies, where tonotopic

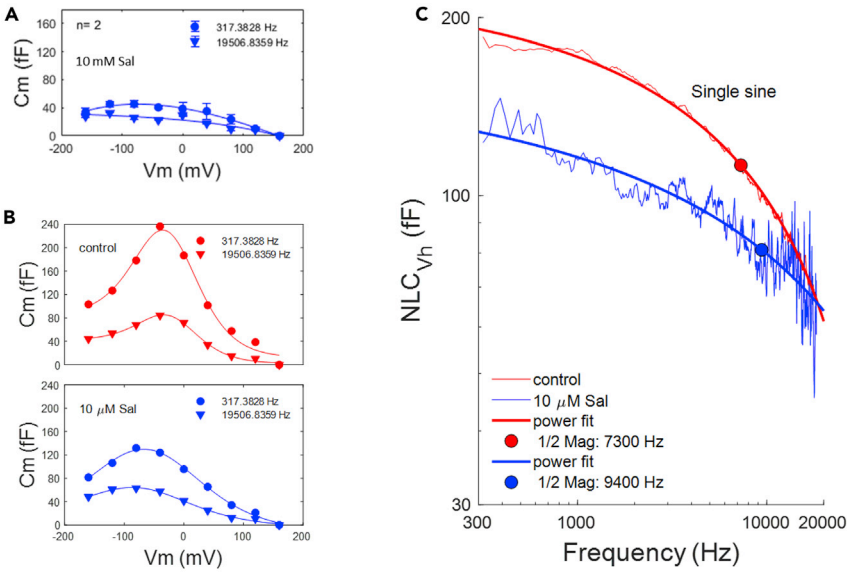

Figure 4. Salicylate Blocks NLC by Reducing Low Frequency Components

Blue color denotes responses after salicylate treatments. Red color denotes control prior to treatment.

(A) NLC is substantially reduced by 10 mM salicylate.

(B) *Top panel*: control before and *bottom panel*: after application of 10 μM salicylate to a single patch to provide partial block of NLC.

(C) The resultant partial inhibition of fit extracted NLC illustrates a low-frequency block, which effectively increases NLC frequency response.

frequency tuning is best (Ashmore et al., 2010). Indeed, OHC eM had been measured in a whole-cell microchamber configuration to work without attenuation beyond 80 kHz at room temperature (Frank et al., 1999), this in spite of initial studies showing more limited charge movement (Gale and Ashmore, 1997a). More recent investigations on whole cells have challenged the concept of OHC high-frequency electromechanical activity, with both NLC and eM exhibiting significant low-pass behavior below 10 kHz (Santos-Sacchi, 2019; Santos-Sacchi et al., 2019; Bai et al., 2019). Our current data on excised and on-cell macro-patch measures of NLC, *where whole-cell mechanical loads on the piezoelectric-like protein prestin are absent,* directly show continuous roll-off of prestin's conformational activity and indicate that attenuation of sensor-charge movement in both mouse and guinea pig is not single Lorentzian in nature, but instead fit well by a power function of frequency. This frequency response is not very different from that of capacitance measures in the GAT1GABA transporter (Lu et al., 1995). Mechanisms that we find to enhance the frequency response of prestin, namely, time-dependence or motor block with salicylate, do not increase its high-frequency behavior, but simply work by reducing the magnitude of low-frequency components. These observations place a severe restraint on the effectiveness of voltage (i.e., receptor potentials) to drive electromechanical responses of the OHC at very high acoustic frequencies where several mammals possess hearing in the 60–160 kHz range. That is, there can be little or no OHC mechanical feedback in the absence of prestin sensor charge movement at high frequencies, assuming that prestin works as an AC motor driven by AC voltage. Interestingly, *in vivo* indications of OHC electromechanical activity in the gerbil obtained with OCT show low pass behavior, as well (Vavakou et al., 2019). Those authors considered the RC filter problem (Santos-Sacchi, 1989), where OHC receptor potentials are expected to be attenuated at very high frequencies by more than 20 dB relative to partition movements, and thus not be able to drive prestin. Our data show that the RC filter problem is inconsequential, in as much as the ability of prestin to follow wide-band voltage perturbations is insufficient in and of itself.

There is no doubt that normal prestin activity is involved in the process that enhances hearing capabilities (Dallos et al., 2008; Santos-Sacchi et al., 2006). Knock-in of prestin mutations that alter its voltage operating range (i.e. V_h) or manipulations of OHC chloride, known to influence prestin activity, are catastrophic to cochlear amplification in the mouse, the latter in a reversible manner. How can a slow motor protein work to enhance high-frequency hearing? Could low pass eM actually be countering low-frequency acoustic responses in order to "highlight" high-frequency input to the cochlea? Intriguing results on basilar

membrane tuning have been obtained in prestin knock-out/in mice that may point to possible mechanisms of OHC action (MelladoLagarde et al., 2008). Alternatively, a rectified DC component of prestin activity (Evans et al., 1991; Santos-Sacchi, 1989) could contribute to effects on high-frequency tuning, as Vavakou et al. (Vavakou et al., 2019) have intimated. Finally, global hydromechanical influences of the OHC may be at play (He et al., 2018). In any case, the long-held cycle-by-cycle hypothesis of cochlear amplification at very high frequencies is directly countered by our present observations.

Limitations of the Study

Ion concentrations in pipette and cell over the timescale of recording are likely fixed; however, conceivably, as in any macro-patch experiment, ion depletion or accumulation on the patched membrane could influence electrical measures.

METHODS

All methods can be found in the accompanying Transparent Methods supplemental file.

SUPPLEMENTAL INFORMATION

Supplemental Information can be found online at https://doi.org/10.1016/j.isci.2019.11.036.

ACKNOWLEDGMENTS

This research was supported by NIH-NIDCD R01DC000273, R01DC016318, and R01DC008130 to J.S.-S.

AUTHOR CONTRIBUTIONS

J.S.-S. designed and performed experiments, analyzed data and wrote the paper. W.T. performed experiments, analyzed data, and edited paper.

DECLARATION OF INTERESTS

The authors declare no conflict of interest.

Received: October 7, 2019
Revised: November 13, 2019
Accepted: November 18, 2019
Published: December 20, 2019

REFERENCES

Ashmore, J., Avan, P., Brownell, W.E., Dallos, P., Dierkes, K., Fettiplace, R., Grosh, K., Hackney, C.M., Hudspeth, A.J., Juelicher, F., et al. (2010). The remarkable cochlear amplifier. Hear. Res. *266*, 1–17.

Ashmore, J.F. (1990). Forward and reverse transduction in the mammalian cochlea. Neurosci. Res. Suppl. *12*, S39–S50.

Bai, J.P., Navaratnam, D., and Santos-Sacchi, J. (2019). Prestin kinetics and corresponding frequency dependence augment during early development of the outer hair cell within the mouse organ of Corti. Sci. Rep. *9*, 16460.

Castellote, M., Mooney, T.A., Quakenbush, L., Hobbs, R., Goertz, C., and Gaglione, E. (2014). Baseline hearing abilities and variability in wild beluga whales (Delphinapterusleucas). J. Exp. Biol. *217*, 1682–1691.

Dallos, P. (2008). Cochlear amplification, outer hair cells and prestin. Curr. Opin. Neurobiol. *18*, 370–376.

Dallos, P., Wu, X., Cheatham, M.A., Gao, J., Zheng, J., Anderson, C.T., Jia, S., Wang, X., Cheng, W.H., Sengupta, S., et al. (2008). Prestin-based outer hair cell motility is necessary for mammalian cochlear amplification. Neuron *58*, 333–339.

Davis, H. (1983). An active process in cochlear mechanics. Hear. Res. *9*, 79–90.

Evans, B.N., Hallworth, R., and Dallos, P. (1991). Outer hair cell electromotility: the sensitivity and vulnerability of the DC component. Hear. Res. *52*, 288–304.

Frank, G., Hemmert, W., and Gummer, A.W. (1999). Limiting dynamics of high-frequency electromechanical transduction of outer hair cells. Proc. Natl. Acad. Sci. U S A *96*, 4420–4425.

Gale, J.E., and Ashmore, J.F. (1994). Charge displacement induced by rapid stretch in the basolateral membrane of the Guinea-pig outer hair cell. Proc. R. Soc. Lond. B Biol. Sci. *255*, 243–249.

Gale, J.E., and Ashmore, J.F. (1997a). An intrinsic frequency limit to the cochlear amplifier. Nature *389*, 63–66.

Gale, J.E., and Ashmore, J.F. (1997b). The outer hair cell motor in membrane patches. Pflugers Arch. *434*, 267–271.

Heffner, H., and Masterton, B. (1980). Hearing in Glires: domestic rabbit, cotton rat, feral house mouse, and kangaroo rat. J. Acoust. Soc. Am. *68*, 1584–1599.

He, W., Kemp, D., and Ren, T. (2018). Timing of the reticular lamina and basilar membrane vibration in living gerbil cochleae. Elife *7*, e37625.

Heffner, R.S., Koay, G., and Heffner, H.E. (2001). Audiograms of five species of rodents: implications for the evolution of hearing and the perception of pitch. Hear. Res. *157*, 138–152.

Iwasa, K.H. (1993). Effect of stress on the membrane capacitance of the auditory outer hair cell. Biophys. J. *65*, 492–498.

Iwasa, K.H., and Kachar, B. (1989). Fast in vitro movement of outer hair cells in an external electric field: effect of digitonin, a membrane permeabilizing agent. Hear. Res. *40*, 247–254.

Kachar, B., Brownell, W.E., Altschuler, R., and Fex, J. (1986). Electrokinetic shape changes of cochlear outer hair cells. Nature *322*, 365–368.

Kakehata, S., and Santos-Sacchi, J. (1995). Membrane tension directly shifts voltage dependence of outer hair cell motility and associated gating charge. Biophys. J. *68*, 2190–2197.

Kakehata, S., and Santos-Sacchi, J. (1996). Effects of salicylate and lanthanides on outer hair cell motility and associated gating charge. J.Neurosci. *16*, 4881–4889.

Lu, C.C., Kabakov, A., Markin, V.S., Mager, S., Frazier, G.A., and Hilgemann, D.W. (1995). Membrane transport mechanisms probed by capacitance measurements with megahertz voltage clamp. Proc. Natl. Acad. Sci. U S A *92*, 11220–11224.

MelladoLagarde, M.M., Drexl, M., Lukashkin, A.N., Zuo, J., and Russell, I.J. (2008). Prestin's role in cochlear frequency tuning and transmission of mechanical responses to neural excitation. Curr. Biol. *18*, 200–202.

Oliver, D., He, D.Z., Klocker, N., Ludwig, J., Schulte, U., Waldegger, S., Ruppersberg, J.P., Dallos, P., and Fakler, B. (2001). Intracellular anions as the voltage sensor of prestin, the outer hair cell motor protein. Science *292*, 2340–2343.

Pollak, G., Henson, O.W., Jr., and Novick, A. (1972). Cochlear microphonic audiograms in the "pure tone" bat Chilonycterisparnelliiparnellii. Science *176*, 66–68.

Rybalchenko, V., and Santos-Sacchi, J. (2003). Allosteric modulation of the outer hair cell motor protein prestin by chloride. In Biophysics of the Cochlea: From Molecules to Models, A. Gummer, ed. (World Scientific Publishing), pp. 116–126.

Santos-Sacchi, J. (1989). Asymmetry in voltage-dependent movements of isolated outer hair cells from the organ of Corti. J.Neurosci. *9*, 2954–2962.

Santos-Sacchi, J. (1990). Fast outer hair cell motility: how fast is fast? In The Mechanics and Biophysics of Hearing, P. Dallos, C.D. Geisler, J.W. Matthews, M.A. Ruggero, and C.R. Steele, eds. (Springer-Verlag), pp. 69–75.

Santos-Sacchi, J. (1991). Reversible inhibition of voltage-dependent outer hair cell motility and capacitance. J. Neurosci. *11*, 3096–3110.

Santos-Sacchi, J. (2019). The speed limit of outer hair cell electromechanical activity. HNO *67*, 159–164.

Santos-Sacchi, J., and Dilger, J.P. (1988). Whole cell currents and mechanical responses of isolated outer hair cells. Hear. Res. *35*, 143–150.

Santos-Sacchi, J., Huang, G.J., and Wu, M. (1997). Mapping the distribution of outer hair cell voltage-dependent conductances by electrical amputation. Biophys. J. *73*, 1424–1429.

Santos-Sacchi, J., Iwasa, K.H., and Tan, W. (2019). Outer hair cell electromotility is low-pass filtered relative to the molecular conformational changes that produce nonlinear capacitance. J. Gen. Physiol. https://doi.org/10.1085/jgp.201812280.

Santos-Sacchi, J., and Navarrete, E. (2002). Voltage-dependent changes in specific membrane capacitance caused by prestin, the outer hair cell lateral membrane motor. Pflugers Arch. *444*, 99–106.

Santos-Sacchi, J., Navarrete, E., and Song, L. (2009). Fast electromechanical amplification in the lateral membrane of the outer hair cell. Biophys. J. *96*, 739–747.

Santos-Sacchi, J., and Song, L. (2014). Chloride-driven electromechanical phase lags at acoustic frequencies are generated by SLC26a5, the outer hair cell motor protein. Biophys. J. *107*, 126–133.

Santos-Sacchi, J., Song, L., Zheng, J., and Nuttall, A.L. (2006). Control of mammalian cochlear amplification by chloride anions. J. Neurosci. *26*, 3992–3998.

Santos-Sacchi, J., and Tan, W. (2018). The frequency response of outer hair cell voltage-dependent motility is limited by kinetics of prestin. J. Neurosci. *38*, 5495–5506.

Sokabe, M., Sachs, F., and Jing, Z.Q. (1991). Quantitative video microscopy of patch clamped membranes stress, strain, capacitance, and stretch channel activation. Biophys. J. *59*, 722–728.

Song, L., and Santos-Sacchi, J. (2010). Conformational state-dependent anion binding in prestin: evidence for allosteric modulation. Biophys. J. *98*, 371–376.

Szymanski, M.D., Bain, D.E., Kiehl, K., Pennington, S., Wong, S., and Henry, K.R. (1999). Killer whale (Orcinus orca) hearing: auditory brainstem response and behavioral audiograms. J. Acoust. Soc. Am. *106*, 1134–1141.

Tunstall, M.J., Gale, J.E., and Ashmore, J.F. (1995). Action of salicylate on membrane capacitance of outer hair cells from the Guinea-pig cochlea. J. Physiol. *485* (Pt 3), 739–752.

Vavakou, A., Cooper, N.P., and van der Heijden, M. (2019). The frequency limit of outer hair cell motility measured in vivo. Elife *8*, e47667.

von Bekesy, G. (1960). Experiments in Hearing (McGraw-Hill).

Walter, J.D., Sawicka, M., and Dutzler, R. (2019). Cryo-EM structures and functional characterization of murine Slc26a9 reveal mechanism of uncoupled chloride transport. Elife *8*, https://doi.org/10.7554/eLife.46986.

Zheng, J., Shen, W., He, D.Z., Long, K.B., Madison, L.D., and Dallos, P. (2000). Prestin is the motor protein of cochlear outer hair cells. Nature *405*, 149–155.

ISCI, Volume *22*

Supplemental Information

Voltage Does Not Drive Prestin (SLC26a5) Electro-Mechanical Activity at High Frequencies Where Cochlear Amplification Is Best

Joseph Santos-Sacchi and Winston Tan

Transparent Methods

OHCs were isolated from guinea pig and mouse as described previously (Santos-Sacchi et al., 2019; Santos-Sacchi and Tan, 2018). Briefly, animals were killed by anesthetic overdose, the cochleas removed and the organ of Corti of the top two coils dissected out. Following 5 minutes of enzymatic digestion with trypsin (0.5mg/ml), the OHCs were isolated by gentle trituration and placed in a petri dish on a Nikon Eclipse TI-2000 microscope for recording. Extracellular solution was (in mM): NaCl 100, TEA-Cl 20, CsCl 20, $CoCl_2$ 2, $MgCl_2$ 1, $CaCl_2$ 1, Hepes 10, pH 7.2. Extracellular solution was in the patch pipette. Macro-patches on the OHC lateral membrane were made near the middle of the cylindrical cell; since prestin density/activity is uniform within the lateral membrane (Dallos et al., 1991; Huang and Santos-Sacchi, 1993), they provide representative information. For the guinea pig on-cell macro-patch approach we used pipette inner diameters of 3.38 +/- 0.20 μm (electrode resistance in bath 1.46 +/- 0.06 MΩ, n=13), with M-coat applied within about 20 μm of the tip to minimize pipette capacitance. Hemispheric estimate of patch surface area was 179 fF. Mouse pipette tip size was smaller at 2.29 +/- 0.024 μm (n=3). In order to establish Gohm seals (5.54 +/- 0.59 GΩ, n=13) we supplemented extracellular solution with 5-7.5 μM Gd^{+3}; we have shown previously that theses low concentrations help to form seals without affecting NLC (Santos-Sacchi and Song, 2016; Santos-Sacchi et al., 2019). **Fig. 1A-D** illustrates our protocol to measure high frequency NLC. Voltage steps from -160 mV to 160 mV were superimposed with an array of voltage chirps. We have previously shown that breakdown of prestin expressing membrane occurs at voltages greater than 300 mV (Navarrete and Santos-Sacchi, 2006). Nevertheless, patches where instabilities of the membrane produced erratic currents at the largest potentials were removed from our data set. An Axon 200B amplifier was used with jClamp software (www.scisoftco.com). An Axon Digidata 1440 was used for digitizing at 10 μs (Nyquist frequency of 50 kHz). Currents were filtered at 10 kHz with a 4-pole Bessel filter. The voltage chirps were generated in the software program jClamp (www.scisoftco.com) using the Matlab logarithmic "chirp" function (10 mV pk; pts=4096; F0=24.4141 Hz; F1=50 kHz; t1=0.04095 s). Subtraction of currents at very depolarized potentials (160 mV) where NLC is absent (Santos-Sacchi and Navarrete, 2002), provided prestin-associated nonlinear currents, absent stray capacitive currents. Subsequently, these subtracted nonlinear membrane currents were used

for dual-sine or single-sine based capacitance estimation by evaluating real and imaginary components of the differential input admittance (Y_{diff}) derived from the subtracted currents (Santos-Sacchi, 2004; Santos-Sacchi et al., 1998). The removal of stray capacitance is required for the application of membrane capacitance algorithms (see below). Briefly, real and imaginary components of the nonlinear membrane admittance at all chirp frequencies were determined by FFT in jClamp, and corrected for the roll-off of recording system admittance (Gillis, 1995). That is, the frequency response of the system, including all components (AD/DA, amplifier and filter) was assessed by placing a small shielded resistor, 10 MΩ, into the head stage input. Stray capacitance was balanced out with amplifier circuitry prior to grounding the resistor. Then, following grounding, voltage chirps (frequency span from 3.05 to 50 kHz, 32768 points at 10 μs clock) were delivered, and currents recorded to provide system admittance. The magnitude and phase of our system response is shown in **Figure S1 A and B**. That system admittance is used to correct experimental data admittance. The necessity for such corrections are shown in **Figure S1 C-D**, where an electrical cell model (Rs: 10 MΩ, Rm: 2 GΩ, and Cm: 1 pF) was analyzed similar to macro-patches, after stray capacitance compensation with amplifier circuitry. It can be seen, for both the dual sine and single sine analysis, that uncorrected responses are aberrant, but following correction for system magnitude and phase (i.e., dividing the complex response admittance by system admittance at each stimulus frequency), the subsequently estimated capacitance is flat at about 1 pF across frequency, regardless of holding potential. Thus, our methodology permits us to measure capacitance with high fidelity out to 20 kHz across holding potentials. We and others have previously used such an approach, though at lower interrogating frequencies, to measure NLC, as well as capacitance associated with synaptic vesicle release (Santos-Sacchi, 2018; Schnee et al., 2011b; Schnee et al., 2011a; Santos-Sacchi et al., 1998).

For the dual sine method, the solution of the standard electrode-cell model is obtained from the admittances at 2 interrogating frequencies (Santos-Sacchi et al., 1998; Santos-Sacchi, 2018), based on the original single sine solution of Pusch and Neher (Pusch and Neher, 1988). The component solutions at harmonic angular frequencies ω_n, where n=0, 1 and $\omega_n=2\pi f_n$, are

$$R_{s_n} = \frac{a_n - \beta}{{a_n}^2 + {b_n}^2 - a_n \beta}$$

$$R_{m_n} = \frac{1}{b}\frac{((a_n - \beta)^2 + {b_n}^2)}{({a_n}^2 + {b_n}^2 - a_n\beta)}$$

$$C_{m_n} = \frac{1}{(\omega_n b_n)}\frac{\left({a_n}^2 + {b_n}^2 - a_n\beta\right)^2}{((a_n - \beta)^2 + {b_n}^2)}$$

where from the measured input admittance Y_{in} we obtain

$$Y_{cell_{\omega_n}} = Y_{in_{\omega_n}} - Y_{stray_{\omega_n}}, n = 0,1$$

$$a_n = Re\left(Y_{cell_{\omega_n}}\right)$$

$$b_n = Im\left(Y_{cell_{\omega_n}}\right)$$

$$c_n = {a_n}^2 + {b_n}^2$$

$$\beta = -0.5 \times \frac{-c_1 + c_0 + \sqrt{{c_1}^2 - 2\,c_1\,c_0 + {c_0}^2 - 4\,a_1 a_0\,c_1 + 4{a_1}^2\,c_0 + 4\,{a_0}^2\,c_1 - 4\,a_0 a_1\,c_0}}{a_1 - a_0}$$

Thus, membrane currents evoked by two voltage frequencies can be used to solve for R_s, R_m and C_m, even in the face of resistive changes, *but only in the absence of stray capacitance*. This applies to measures of patch capacitance, as well. We report on C_m measures derived from f_n, where n=0.

For single sine analysis, capacitance was estimated from the imaginary component of the admittance, $C_m = Im(Y_{diff})/\omega$, where $\omega = 2\pi f$, after minimizing the real component of admittance by rotating the phase angle of the complex admittance. Single and dual sine frequency response estimates were essentially the same (for example, see **Figure S1 D and F**).

To extract NLC at each frequency, we fit V_m-C_m data to the following *eq. 1* (Santos-Sacchi and Navarrete, 2002). This equation extracts NLC based on a 2-state charge movement (Boltzmann) model, which predicts symmetrical NLC on either side of V_h. In fact, measured membrane capacitance in OHCs or prestin-expressing heterologous cells is greater at hyperpolarized potentials than at depolarized potentials. This voltage-dependent sigmoidal offset is removed by the fit (see **Fig. 1H**). The equation has been routinely used to evaluate NLC (Santos-Sacchi and Song, 2014; Homma and Dallos, 2011; Duret et al., 2017; Chessum et al., 2018; Harasztosi and Gummer, 2016).

eq. 1

$$C_m = Q_{max}\,\frac{ze}{kT}\,\frac{b}{(1+b)^2} + \frac{\Delta C_{sa}}{(1+b^{-1})} + C_0$$

where

$$b = exp\left(\frac{-ze(V_m - V_h)}{kT}\right)$$

Q_{max} is the maximum nonlinear charge moved, V_h is voltage at peak capacitance or equivalently, at half maximum charge transfer, V_m is membrane potential, z is valence, e is electron charge, k is Boltzmann's constant, and T is absolute temperature. C_0 is defined as the capacitance of the membrane when all motors are in their compact state, the minimum membrane capacitance; ΔC_{sa} is the maximum increase in capacitance that occurs when all motors change from compact to expanded state, each motor contributing a unit response of δC_{sa}.

Data are presented as mean +/- standard error (SE). Data points from previous publications were extracted from plots using the application Grabit (written by Jiro Doke) in Matlab.

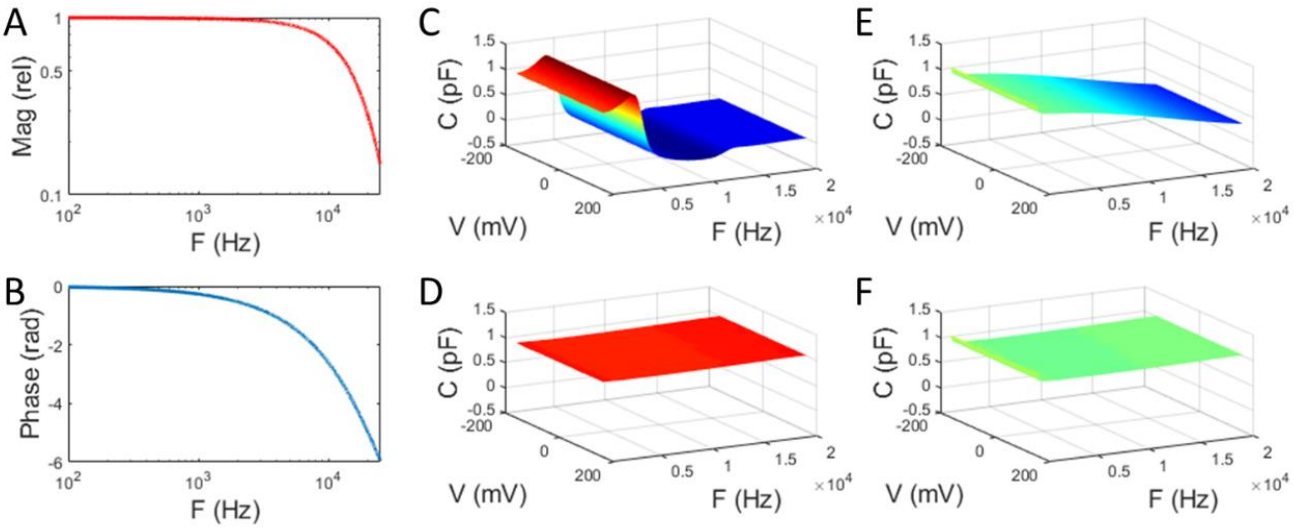

Figure S1 Requirement to correct for the frequency response of the patch clamp system prior to capacitance estimation, Related to Figure 1 and 2. A) Magnitude and B) phase of the system. Determination is detailed in the Methods. In C-D, a model electrical patch (R_s: 10 MΩ, R_m: 2GΩ, C_m: 1 pF) is used to confirm proper system performance. C,D) illustrate capacitance measures utilizing dual sine analysis and E,F) using single sine analysis as detailed in Methods. In C) and E) capacitance measures are not corrected for system frequency response. Responses are aberrant. In D) and F) corrections are made to the measured model patch admittance based on measured system admittance. Following corrections, capacitance measures are flat out to 20 kHz, across holding potentials of -160 to 160 mV.

References

Chessum, L., Matern, M. S., Kelly, M. C., Johnson, S. L., Ogawa, Y., Milon, B., McMurray, M., Driver, E. C., Parker, A., Song, Y., Codner, G., Esapa, C. T., Prescott, J., Trent, G., Wells, S., Dragich, A. K., Frolenkov, G. I., Kelley, M. W., Marcotti, W., Brown, S. D. M., Elkon, R., Bowl, M. R. & Hertzano, R. 2018. Helios is a key transcriptional regulator of outer hair cell maturation. *Nature*, 563(7733)**,** pp 696-700.

Dallos, P., Evans, B. N. & Hallworth, R. 1991. Nature of the motor element in electrokinetic shape changes of cochlear outer hair cells. *Nature*, 350(6314)**,** pp 155-157.

Duret, G., Pereira, F. A. & Raphael, R. M. 2017. Diflunisal inhibits prestin by chloride-dependent mechanism. *PLoS One,* 12(8)**,** pp e0183046.

Gillis, K. D. 1995. Techniques for Membrane Capacitance Measurements. *In:* Sakmann, B. & Neher, E. (eds.) *Single Channel Recording.* New York: Plenum Press.

Harasztosi, C. & Gummer, A. W. 2016. The chloride-channel blocker 9-anthracenecarboxylic acid reduces the nonlinear capacitance of prestin-associated charge movement. *Eur J Neurosci,* 43(8)**,** pp 1062-74.

Homma, K. & Dallos, P. 2011. Evidence that prestin has at least two voltage-dependent steps. *J.Biol.Chem.,* 286(3)**,** pp 2297-2307.

Huang, G. & Santos-Sacchi, J. 1993. Mapping the distribution of the outer hair cell motility voltage sensor by electrical amputation. *Biophys.J.,* 65(5)**,** pp 2228-2236.

Navarrete, E. G. & Santos-Sacchi, J. 2006. On the effect of prestin on the electrical breakdown of cell membranes. *Biophys.J.,* 90(3)**,** pp 967-974.

Pusch, M. & Neher, E. 1988. Rates of diffusional exchange between small cells and a measuring patch pipette. *Pflugers Arch.,* 411(2)**,** pp 204-211.

Santos-Sacchi, J. 2004. Determination of cell capacitance using the exact empirical solution of dY/dCm and its phase angle. *Biophys.J.,* 87(1)**,** pp 714-727.

Santos-Sacchi, J. 2018. High frequency measures of OHC nonlinear capacitance (NLC) and their significance: Why measures stray away from predictions. *AIP Conference Proceedings,* 1965(1)**,** pp 060004-1–060004-5.

Santos-Sacchi, J., Iwasa, K. H. & Tan, W. 2019. Outer hair cell electromotility is low-pass filtered relative to the molecular conformational changes that produce nonlinear capacitance. *J Gen Physiol,* jgp.201812280. doi: 10.1085/jgp.201812280(

Santos-Sacchi, J., Kakehata, S. & Takahashi, S. 1998. Effects of membrane potential on the voltage dependence of motility-related charge in outer hair cells of the guinea-pig. *J.Physiol,* 510 (Pt 1)(225-235.

Santos-Sacchi, J. & Navarrete, E. 2002. Voltage-dependent changes in specific membrane capacitance caused by prestin, the outer hair cell lateral membrane motor. *Pflugers Arch.,* 444(1-2)**,** pp 99-106.

Santos-Sacchi, J. & Song, L. 2014. Chloride and Salicylate Influence Prestin-dependent Specific Membrane Capacitance. *Journal of Biological Chemistry,* 289(15)**,** pp 10823-10830.

Santos-Sacchi, J. & Song, L. 2016. Chloride anions regulate kinetics but not voltage-sensor Qmax of the solute carrier SLC26a5. *Biophysical Journal,* 110(1-11.

Santos-Sacchi, J. & Tan, W. 2018. The Frequency Response of Outer Hair Cell Voltage-Dependent Motility Is Limited by Kinetics of Prestin. *J Neurosci,* 38(24)**,** pp 5495-5506.

Schnee, M. E., Santos-Sacchi, J., Castellano-Munoz, M., Kong, J.-H. & Ricci, A. J. 2011a. Calcium-Dependent Synaptic Vesicle Trafficking Underlies Indefatigable Release at the Hair Cell Afferent Fiber Synapse. *Neuron,* 70(2)**,** pp 326-338.

Schnee, M. E., Santos-Sacchi, J., Castellano-Munoz, M., Kong, J. H. & Ricci, A. J. 2011b. Tracking vesicle fusion from hair cell ribbon synapses using a high frequency, dual sine wave stimulus paradigm. *Communicative & Integrative Biology,* 4(6)**,** pp 785-787.